MNRAS **000**, 1–11 (0000) Preprint 3 October 2016 Compiled using MNRAS LATEX style file v3.0

Light or heavy supermassive black hole seeds: the role of internal rotation in the fate of supermassive stars

Davide Fiacconi[1,⋆] and Elena M. Rossi[2,†]
[1]*Center for Theoretical Astrophysics and Cosmology, Institute for Computational Science, University of Zurich, Winterthurerstrasse 190, CH-8057 Zürich, Switzerland*
[2]*Leiden Observatory, Leiden University, PO Box 9513, 2300 RA, Leiden, the Netherlands*

arXiv:1604.03936v2 [astro-ph.HE] 29 Sep 2016

3 October 2016

ABSTRACT

Supermassive black holes are a key ingredient of galaxy evolution. However, their origin is still highly debated. In one of the leading formation scenarios, a black hole of ~ 100 M$_\odot$ results from the collapse of the inner core of a supermassive star ($\gtrsim 10^{4-5}$ M$_\odot$), created by the rapid accumulation ($\gtrsim 0.1$ M$_\odot$ yr^{-1}) of pristine gas at the centre of newly formed galaxies at $z \sim 15$. The subsequent evolution is still speculative: the remaining gas in the supermassive star can either directly plunge into the nascent black hole, or part of it can form a central accretion disc, whose luminosity sustains a surrounding, massive, and nearly hydrostatic envelope (a system called a "quasi-star"). To address this point, we consider the effect of rotation on a quasi-star, as angular momentum is inevitably transported towards the galactic nucleus by the accumulating gas. Using a model for the internal redistribution of angular momentum that qualitative matches results from simulations of rotating convective stellar envelopes, we show that quasi-stars with an envelope mass greater than a few 10^5 M$_\odot \times$ (black hole mass/100 M$_\odot$)$^{0.82}$ have highly sub-keplerian gas motion in their core, preventing gas circularisation outside the black hole's horizon. Less massive quasi-stars could form but last for only $\lesssim 10^4$ years before the accretion luminosity unbinds the envelope, suppressing the black hole growth. We speculate that this might eventually lead to a dual black hole seed population: (i) massive ($> 10^4$ M$_\odot$) seeds formed in the most massive ($> 10^8$ M$_\odot$) and rare haloes; (ii) lighter ($\sim 10^2$ M$_\odot$) seeds to be found in less massive and therefore more common haloes.

Key words: black hole physics – accretion, accretion discs – galaxies: nuclei – cosmology: early Universe – methods: analytical

1 INTRODUCTION

During the last ten years or so, observations have unambiguously proved the existence of supermassive black holes accreting at the centre of bright quasars at redshifts $z \gtrsim 6$ with masses in excess of 10^9 M$_\odot$ (Fan et al. 2006; Willott et al. 2010; Mortlock et al. 2011; Wu et al. 2015). Despite that those objects are not perhaps representative of the entire population of supermassive black holes at $z \gtrsim 6$ (e.g. Treister et al. 2013; Weigel et al. 2015), they represent a challenge for many theoretical models that attempt to describe the formation of the first black hole seeds. Indeed, black hole seeds originating both as the leftovers of the first population (PopIII) stars (with masses $\lesssim 100$ M$_\odot$; Madau & Rees 2001; Tanaka & Haiman 2009), and as the product of dynamical processes at the centre of primordial nuclear star cluster (with masses $\lesssim 1000$ M$_\odot$; Quinlan & Shapiro 1990; Devecchi & Volonteri 2009; Devecchi et al. 2012), are not expected to grow fast enough to reach $\sim 10^9$ M$_\odot$ by $z \sim 6$ (e.g. Johnson & Bromm 2007; Pelupessy et al. 2007; Milosavljević et al. 2009), unless they experience prolonged periods of super-Eddington accretion (e.g. Madau et al. 2014; Volonteri et al. 2015).

A possible way out is to allow for the existence of massive black hole seeds ($\sim 10^4 - 10^5$ M$_\odot$) that can grow sub-Eddington and still match the masses of the quasars at $z \sim 6$. This is achieved by the so called 'direct collapse' scenario, according to which massive clouds ($\sim 10^6 - 10^7$ M$_\odot$) of pristine gas can collapse almost isothermally at the centre of protogalactic, HI-cooling haloes (i.e. with virial temperature $T_{\rm vir} \gtrsim 10^4$ K; e.g. Bromm & Loeb 2003; Begelman et al. 2006; Lodato & Natarajan 2006; Latif et al. 2013a; Choi et al. 2013, 2015). During the collapse, fragmentation can be avoided by dissociating H_2 (the main coolant in absence of metals) through the irradiation of Lyman-Werner photons coming from nearby, star-forming galaxies (e.g. Dijkstra et al. 2014; Regan et al. 2014; Agarwal et al. 2015), while supersonic turbulence and non-axisymmetric perturbations can remove angular mo-

⋆ E-mail: fiacconi@physik.uzh.ch
† E-mail: emr@strw.leidenuniv.nl

© 0000 The Authors

mentum from the collapsing gas and suppress fragmentation further (Begelman & Shlosman 2009; Choi et al. 2013, 2015; Mayer et al. 2015).

However, even if the concurrency of all the processes above can be attained and it leads to the onset of the gravitational collapse, it is still unclear how the black hole seed would actually form. The expectation is that the collapse proceeds almost isothermally at ~ 8000 K (as set by HI-line cooling) until a supermassive protostars forms at the fragmentation scale $\sim 10^5 - 10^6$ M$_\odot$, quickly accreting at $\sim 0.1 - 1$ M$_\odot$ yr^{-1} (Hosokawa et al. 2012, 2013). After exhausting nuclear reactions, the central core of a supermassive star $\gtrsim 10^{4-5}$ M$_\odot$ is expected to collapse in a ~ 100 M$_\odot$ embryo black hole (Begelman 2010; Hosokawa et al. 2013) because of general relativistic radial instability (Baumgarte & Shapiro 1999; Shibata & Shapiro 2002). The black hole is surrounded by most of the mass of the original envelope which is still contracting on a longer dynamical timescale. It is unclear what happens next. Possibly, the infalling gas retains enough angular momentum to build some kind of an accretion disc around the black hole at the centre of the envelope. This structure can reach the equilibrium where the accretion luminosity is used to sustain the massive envelope against its own self-gravity, i.e. a *quasi-star* (Begelman et al. 2008; Ball et al. 2011; Dotan et al. 2011; Fiacconi & Rossi 2016, hereafter Paper I). Therefore, a necessary ingredient for a quasi-star is the presence of a central accretion disc. It forms within the sphere of influence of the black hole ($\ll$ than the quasi-star radius) and it is able to convectively transport outward into the hydrostatic envelope the potential energy liberated through accretion.

In this way, quasi-stars can quickly grow their central black holes to $\sim 10^4$ M$_\odot$ at (or above) the Eddington rate for the whole envelope, although strong outflows can limit the black hole growth (Dotan et al. 2011; Paper I). At the same time, the envelope keeps accreting mass from the environment. Whether such accretion proceeds directly through filaments or from a protogalactic disc, the gas likely transports some amount of angular momentum that is transferred to the quasi-star and redistributed within it. Quasi-stars are then expected to rotate, possibly faster on the equatorial plane than on the poles if they are embedded in a disc.

Rotation may have a few effects on the evolution of quasi-stars. In analogy with normal stars, it could modify the internal structure of the quasi-star (e.g. Palacios et al. 2006; Eggenberger et al. 2010; Brott et al. 2011; Ekström et al. 2012), or it can stabilise the object against general relativistic instabilities, unless too massive ($\gtrsim 10^8$ M$_\odot$; Fowler 1966). Finally, a crucial feature that depends on the internal redistribution of angular momentum is the ability of the gas to circularise and to form an accretion disc. Here we explore whether the conditions for a disc to form are typically met in steady-rotating quasi-stars and we find that in most of the parameter space the answer is negative. Although this result might be sensitive to environmental conditions as well as to details of the convective structures, it opens in principle the possibility of directly forming massive seeds, without the intermediate stage of a quasi-star.

This paper is organised as follows. In Section 2, we present our analytical model to describe the differential rotation within quasi-stars and we calculate the angular velocity profiles, finding that the angular momentum at the boundary of the accretion region is typically much less than a percent of the Keplerian angular momentum at the same location. Before concluding, we discuss in Section 3 the speculative implications of our work, cautioning at the same time about the limitations of our approach.

2 THE MODEL OF ROTATING QUASI-STARS

2.1 Quasi-stars as loaded polytropes

The hydrostatic structure of a quasi-star is constituted by a radiation-dominated, convective envelope, surrounded by a thin, radiative layer (Begelman et al. 2008; Ball et al. 2011; Dotan et al. 2011; Paper I). Since the envelope represents the majority of the mass and volume of a quasi-star and convective regions can be described accurately by an adiabatic temperature gradient, a quasi-star can be modelled as a polytropic gas with index $n = 3$. A polytropic gas is characterised by a barotropic equation of state $P(\rho) = P_\mathrm{c}(\rho/\rho_\mathrm{c})^\gamma$, where P_c and ρ_c are the central pressure and density, respectively, and the adiabatic index $\gamma = 1 + 1/n = 4/3$ for a radiation-dominated gas. Polytropes are regular solutions of the Lane-Emden equations with inner boundary conditions in the standard dimensionless density and mass variables $\Theta_\mathrm{c} = \Theta(0) = 1$ and $\phi_\mathrm{c} = \phi(0) = 0$. When $n < 5$, they extend up to the dimensionless radius $\xi_\star = r_\star/\alpha$, where $\Theta_\star = \Theta(\xi_\star) = 0$ and α is the standard radial normalisation, and they enclose a total, finite mass $M_\star = 4\pi\rho_\mathrm{c}\alpha^3\phi_\star$ (e.g. Ball et al. 2012).

Additionally, quasi-stars are characterised by the presence of a central black hole of mass $M_\bullet$. We can model this feature by changing the inner boundary conditions: we assume that within the radius r_0, the enclosed mass is $M(r_0) = M_\bullet$ and that the density and the pressure are normalised to the values ρ_0 and P_0 at r_0, respectively. The radius r_0 is the size of the gravitational sphere of influence of the black hole and is typically of the order of its Bondi radius r_B:

$$r_0 = b r_\mathrm{B} = b\frac{GM_\bullet}{2c_{\mathrm{s},0}^2}, \tag{1}$$

where $c_{\mathrm{s},0}^2 = \gamma P_0/\rho_0$ and b is a numerical constant of the order of few. In terms of dimensionless quantities, the new boundary conditions at $\xi_0 = r_0/\alpha$ are $\Theta(\xi_0) = \Theta_0 = 1$ and $\phi_0 = \phi(r_0) = M_\bullet/(4\pi\rho_0\alpha^3)$. A polytropic solution with non-zero central mass (i.e. with the latter boundary conditions) is called *loaded polytrope* (Huntley & Saslaw 1975). Throughout the rest of the paper, we use loaded polytropes to model the internal, hydrostatic structure of a quasi-stars assuming $n = 3$.

We note that ξ_0 and ϕ_0 are not independent, but they are related by:

$$\xi_0 = \frac{3b}{2}\phi_0. \tag{2}$$

Therefore, the boundary conditions can be fully determined by choosing a value for ϕ_0. In turn, this is related through the Lane-Emden equation to the total mass of the envelope $\phi_\star$. This relation is shown in Figure 1 in terms of the the mass ratio $q \equiv M_\bullet/M_\star = \phi_0/\phi_\star$ as a function of ϕ_0 for different values of b. The mass ratio q has always a maximum at $\phi_0 = \tilde{\phi}_0$. This occurrence has been described in details by Ball et al. (2012) as a generalisation of a Schönberg-Chandrasekhar-like limit for polytropic envelopes surrounding a central core (Schönberg & Chandrasekhar 1942). Quasi-stars have typically $q < 10^{-2}$ (Paper I). Solutions on the $\phi_0 > \tilde{\phi}_0$ branch are unphysical because they reach zero mass before zero radius. Acceptable solutions lie on the $\phi_0 < \tilde{\phi}_0$ branch, where the dependency on b becomes very weak. On this branch, we find empirically $\phi_0 \approx 2q$, as shown in Figure 1. From this relation, we can build any solution as follows. First, we choose a value of q, typically between $\sim 10^{-4}$ and $\sim 10^{-2}$. This maps to the value of ϕ_0 necessary to set the boundary conditions and specify $\phi_\star$. We can then rescale the dimensionless solution with a specified q to

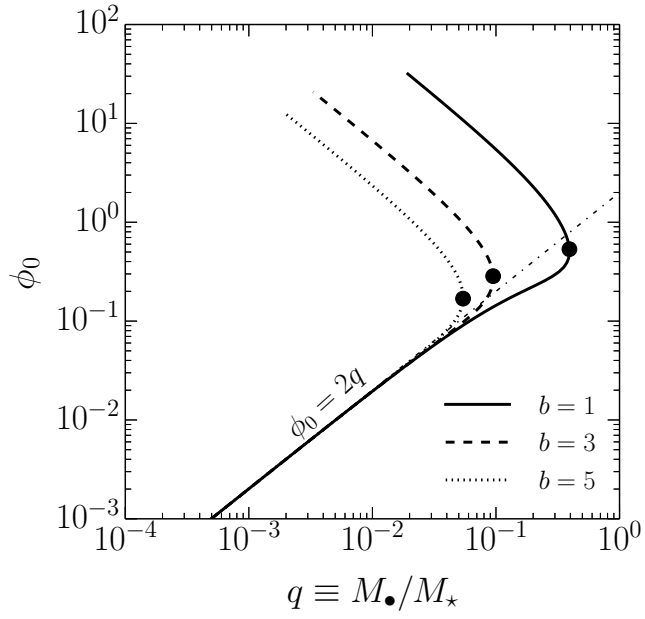

Figure 1. Relation between the mass ratio $q = M_\bullet/M_\star = \phi_0/\phi_\star$ and the dimensionless black hole mass ϕ_0. Continuous, dashed and dotted lines show the case $b = 1$, $b = 3$ and $b = 5$, respectively. The black dots show the position of the limiting mass ratio q. The lower branch ($\phi_0 < 0.1$) is the only one that gives physical solutions (see the text) and it almost does not depend on b. The dash-dotted line shows the relation $\phi_0 = 2q$.

any solution in physical units by specifying the central black hole mass $M_\bullet$ and the pressure P_0. The density ρ_0 can then be obtained as:

$$\rho_0 = \left[\frac{(n+1)^3}{4\pi G^3}\right]^{1/4} \frac{\phi_0^{1/2} P_0^{3/4}}{M_\bullet^{1/2}} \approx \approx 1.2 \times 10^{-5}\, q^{1/2}\, p_{0,8}^{3/4}\, m_\bullet^{-1/2}\ \mathrm{g\ cm^{-3}}, \quad (3)$$

where we use $n = 3$, $M_\bullet = m_\bullet\ \mathrm{M}_\odot$, and $\phi_0 \approx 2q$. We discuss the limitations of this simplified treatment of the interior of quasi-stars in Section 3.2.

2.2 Differential rotation inside quasi-stars

In a recent series of papers, Balbus and collaborators have developed a theory to describe the convective zone in the Sun (Balbus et al. 2009; Balbus & Weiss 2010; Balbus & Latter 2010; Balbus et al. 2012; Balbus & Schaan 2012). Their model successfully reproduces the isorotation contours within the solar convective zone and the tachocline from the helioseismology data of the Global Oscillation Network Group (GONG). Here, we review the main features of the model and we then apply it to quasi-stars, mostly following Balbus et al. (2009) and Balbus & Weiss (2010). We also verify in Section 3.2 the applicability of this model to the quasi-star case.

We consider an azimuthally rotating, convective gas flow (generically a star) in spherical coordinates (r, θ, ϕ), where r is the radial distance from the centre, θ is the colatitude angle and ϕ is the azimuthal angle. The flow is symmetric with respect to the rotation axis, i.e. the thermodynamic variables characterising it, such as the density ρ, the pressure P and the specific entropy s, do not depend on ϕ, but they generally depend on r and θ. The only velocity component is the azimuthal velocity $v_\phi = r\ \sin\theta\ \Omega(r,\theta)$, where $\Omega(r,\theta)$ is the angular velocity. We neglect any departure from sphericity, implicitly assuming slow rotation. Such a flow in steady state is described by the following Euleur equations (r- and θ-component, respectively, while the azimuthal component is $0 = 0$):

$$\begin{cases} -\frac{1}{\rho}\frac{\partial P}{\partial r} - \frac{\partial \Phi}{\partial r} = 0, \\ \frac{v_\phi^2 \cot\theta}{r} - \frac{1}{\rho}\frac{\partial P}{\partial \theta} - \frac{1}{r}\frac{\partial \Phi}{\partial \theta} = 0, \end{cases} \quad (4)$$

where Φ is the gravitational potential. Note that in the radial direction we neglect the (weak) centrifugal force[1]. By taking the ϕ-component of the curl of the Euler equations (equation 4), and dropping terms proportional to $\partial P/\partial\theta \ll \partial P/\partial r$, we obtain the thermal wind equation (Kitchatinov & Ruediger 1995; Thompson et al. 2003; Balbus et al. 2009; Balbus & Weiss 2010; Balbus et al. 2012):

$$\frac{\partial \Omega^2}{\partial r} - \frac{\tan\theta}{r}\frac{\partial \Omega^2}{\partial \theta} = \frac{1}{\gamma\, r^2\, \sin\theta\, \cos\theta}\frac{\mathrm{d}\Phi}{\mathrm{d}r}\frac{\partial \sigma}{\partial \theta}, \quad (5)$$

where we have introduced the dimensionless entropy function:

$$\sigma = \log\left[\frac{P}{P_0}\left(\frac{\rho}{\rho_0}\right)^{-\gamma}\right], \quad (6)$$

which is proportional to (or monotonically dependent on) s. Equation (5) neglects the contribution from convective turbulence to the velocity field (it is in fact a time-averaged description of the flow) and it is not valid for highly magnetised stars, but a weak magnetic field can be accommodated (Balbus 2009).

Let us now introduce the *residual* entropy: the azimuthally averaged entropy profile left, after the radial profile σ_r has been subtracted off:

$$\sigma'(r,\theta) = \sigma - \sigma_r(r). \quad (7)$$

Since equation (5) depends on σ exclusively through its θ derivative, the differential profile $\Omega(r,\theta)$ could be determined after knowing σ', regardless of σ_r. Convection in a non-rotating star establishes a stable entropy radial profile σ_r, as a result of an equilibrium reached between central stellar heating and heat transport. Convective cells moves on average along the radial direction. If now a small amount of rotation is added, the convective cells will tend, on average, to drift towards surfaces of constant angular rotation. This is because differential rotation tends to confine the flow in sheet of constant Ω. This assumes of course that the rotational surfaces can effectively interact with the convective cells during their lifetime, which is reasonable if they are long lasting structures. In the presence of a relative small degree of rotation, we can therefore argue that σ_r is similar to that established in a non-rotating star, while $\sigma'(r,\theta)$ is a small departure from σ_r, closely connected to the differential rotational profile within the star. Following Balbus et al. (2009), we assume, $\sigma' = f(\Omega^2)$ which implies that surfaces of constant residual entropy coincide with surfaces of constant angular velocity. Though still not unambiguously demonstrated, this conjecture provides remarkable results when used to describe the solar convective zone (Balbus & Latter 2010; Balbus et al. 2012;

[1] In fact, this approximation is only necessary to derive equation (5) *after* the ϕ-component of the curl of those Euler equations has been taken. For clarity, however, we already drop the centrifugal force at this early step.

Balbus & Schaan 2012). In addition, it is also supported, at least qualitatively, by the results of hydrodynamical simulations showing similarity between constant Ω and σ' contours (Miesch et al. 2006; see also figure 2 from Balbus et al. 2009).

With this relation, $\sigma' = f(\Omega^2)$, equation (5) can be rewritten as:

$$\frac{\partial \Omega^2}{\partial r} - \left(\frac{\tan\theta}{r} + \frac{f'}{\gamma\, r^2\, \sin\theta\, \cos\theta} \frac{\mathrm{d}\Phi}{\mathrm{d}r} \right) \frac{\partial \Omega^2}{\partial \theta} = 0, \quad (8)$$

where $f' = \mathrm{d}\sigma'/\mathrm{d}\Omega^2$. The above equation has the form $\boldsymbol{u} \cdot \nabla \Omega^2 = 0$, where $\boldsymbol{u}$ is the vector tangential to the surfaces of constant Ω (i.e. it is their "velocity" vector). Such surfaces $\boldsymbol{\zeta} = (r, \theta(r))$ can be obtained by integrating the ordinary differential equation $\dot{\boldsymbol{\zeta}} = \boldsymbol{u}$ (where $\dot{}$ indicates the derivative with respect to any dummy parameter). More practically, one divides the polar and radial component of that vectorial equation and obtains the following single equation:

$$\frac{\mathrm{d}\theta(r)}{\mathrm{d}r} = -\frac{\tan\theta}{r} - \frac{f'}{\gamma\, r^2\, \sin\theta\, \cos\theta} \frac{\mathrm{d}\Phi(r)}{\mathrm{d}r}. \quad (9)$$

If we recall that f' depends only on Ω^2 and that equation (9) describes surfaces of constant Ω^2, we can finally integrate the above equation considering f' as constant:

$$r^2 \sin^2\theta = A - \frac{2f'}{\gamma}\Phi(r), \quad (10)$$

where A is an integration constant. These iso-Ω^2 surfaces are the characteristics of equation (8). Note that on each surface, f' can assume a different constant value.

We can determine the constant A by specifying a starting position for each characteristic. We take the position $(R_\star, \theta_\star)$ at the surface of a spherical star with radius $R_\star$ and we obtain:

$$r^2 \sin^2\theta = R_\star^2 \sin^2\theta_\star - \frac{2f'}{\gamma}(\Phi(r) - \Phi(R_\star)), \quad (11)$$

where now $f' = f'(\Omega(R_\star, \theta_\star))$ has to be specified and the internal structure of the star influences the result through Φ. The curves described by equation (11) are constant Ω contours, therefore they can be used to reconstruct the 2-dimensional $\Omega(r, \theta)$ by assigning a value of Ω at a given radius. Specifically, we will supply $\Omega_\star(\theta_\star)$ at $R_\star$. We can then isolate $\theta_\star(r, \theta)$ from equation (11) and obtain $\Omega(r, \theta) = \Omega_\star(\theta_\star(r, \theta))$.

We can now use this method to explicitly calculate the internal differential rotation of quasi-stars, once we specify their internal structure. Since we describe quasi-stars as loaded polytropes (see Section 2.1), we can integrate the equation of hydrostatic equilibrium between r and $R_\star$ for a polytropic equation of state and obtain:

$$\Phi(r) - \Phi(R_\star) = -\frac{c_\mathrm{s}^2}{\gamma - 1} = -3\, c_{\mathrm{s},0}^2\, \Theta_3(r; q), \quad (12)$$

where $c_{\mathrm{s},0}^2 = \gamma P_0/\rho_0$ is the sound speed at r_0, $\Theta_3(r; q)$ is the loaded polytrope solution for $n = 3$ and a given q, and $\gamma = 4/3$. Substituting equation (12) into equation (11), we finally get:

$$\sin^2\theta_\star = \left(\frac{r}{R_\star}\right)^2 \sin^2\theta - \beta\, \Theta_3(r; q), \quad (13)$$

where we define:

$$\beta = \frac{9 c_{\mathrm{s},0}^2 f'}{2 R_\star^2}. \quad (14)$$

There is still a quantity that has remained general in our treatment, namely $f'(\Omega^2)$. Unfortunately, we do not know a priori its functional form, and only hydrodynamical simulations of global 3D convection could clarify this point. However, to avoid unnecessary mathematical complication at this stage, we assume the simplest functional form, i.e. a global constant for f'. This simple choice is also motivated by the lack of any observational constraint; yet, such a choice is quite effective for the case of the Sun (Balbus & Latter 2010; Balbus et al. 2012). However, we need to use additional reasonable arguments to constrain in our case the constant parameter β, that directly depends on f' through equation (14).

First, we expect $\beta < 0$ (i.e. $f' < 0$, like in the convective envelope of the Sun), since this implies slower rotating poles with respect to the equatorial regions. This configuration may naturally comes about when quasi-stars are fed by protogalactic discs near the equator, i.e. angular momentum is injected by the infalling material near the equator and has to be redistributed from there to the poles. Finally, we can also estimate the value of $|\beta|$ by recalling that σ' is a small perturbation on the otherwise spherically symmetric entropy profile σ_r which arises when the star rotates:

$$\sigma' \sim \frac{T_\mathrm{rot}}{U} \sim \frac{R_\star^2 \Omega^2}{c_{\mathrm{s},0}^2}, \quad (15)$$

where $T_\mathrm{rot} \sim M_\star R_\star^2 \Omega^2$ and $U \sim M_\star c_{\mathrm{s},0}^2$ are the rotational kinetic energy and the gaseous internal energy of the star, respectively. Therefore, $f' \sim \sigma'/\Omega^2 \sim R_\star^2/c_{\mathrm{s},0}^2$ implies that $|\beta| \sim 9/2 \sim$ a few. Although this simple line of reasoning does not prove that f' should be constant, it provides a gross estimate of the value of $|\beta|$ *if* f' is assumed to be constant. However, we show in Section 2.3 that the exact value of $|\beta|$ has a weak impact on our final conclusions and we discuss the limitations of our approach in Section 3.2.

2.3 Angular velocity structure of quasi-stars

To explicitly calculate the differential rotation within a quasi-star, we need to specify the boundary conditions of the problem, i.e. the differential rotation at the surface $\Omega_\star(\theta_\star)$. We use a simple parametrisation of the form:

$$\Omega_\star(\theta_\star) = \omega_\star(1 + \delta\omega \sin^2\theta_\star), \quad (16)$$

where $\omega_\star$ is the polar rotation, limited by the Keplerian velocity of the star $\Omega_{\mathrm{K},\star}$, and $\delta\omega$ is the relative, fractional excess of rotation at the equator, with the limit $0 < \delta\omega < \epsilon^{-1} - 1$, where $\epsilon = \omega_\star/\Omega_{\mathrm{K},\star} < 1$. This parametrisation of the differential rotation has been used to describe the Sun as well as other stars, with typical values $\delta\omega \sim 0.1$ (e.g. Balbus et al. 2009; Reinhold et al. 2013).

Figure 2 shows the angular velocity profiles and maps for a reference quasi-star with $q = 10^{-3}$ (e.g. a massive quasi-star with $M_\bullet = 10^3\ \mathrm{M}_\odot$ and $M_\star = 10^6\ \mathrm{M}_\odot$), $\epsilon = 0.3$ and $\delta\omega = 0.2$ (i.e. rotating at $0.36\ \Omega_{\mathrm{K},\star}$ at the equator, with a differential velocity of 20% between the equator and the poles), and we vary the value of $|\beta|$ between 1 and 16. The upper-left panel (sub-panel (a)) shows the radial profile of the θ-averaged angular velocity $\langle\Omega\rangle$ (normalised by $\Omega_{\mathrm{K},\star}$), highlighting its behaviour at small radii. Initially, $\langle\Omega\rangle$ grows from the surface of the star inward for most of the stellar volume till $\sim 0.1 R_\star$. This growth is accentuated for larger values of $|\beta|$. Within $0.1 R_\star$, $\langle\Omega\rangle$ remains almost constant, assuming a solid-body-like rotation law and following the central density of the gas that also starts to flatten in a central core. However, the angular velocity deviates from constant within $0.005\ R_\star$ (or $\sim 20\, r_0$) because of the presence of the central black hole, steepening at smaller radii. The typical trend is $\propto r^{-\zeta}$, with $\zeta \sim 0.2 - 0.6$, increasing with $|\beta|$. We compare $\langle\Omega\rangle$ with the Keplerian angular

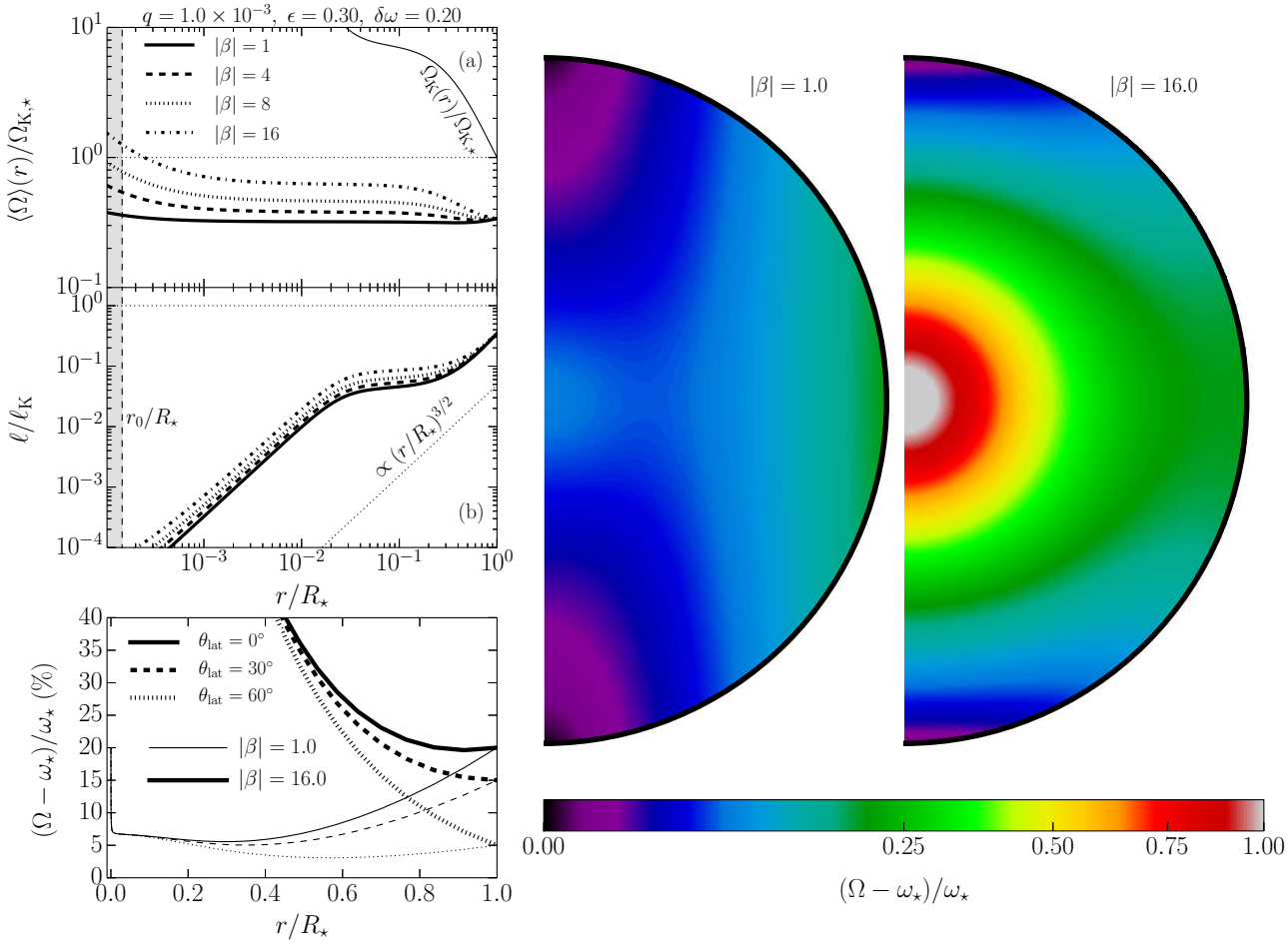

Figure 2. Angular velocity for a quasi-star model characterised by $q = 10^{-3}$, $\epsilon = 0.3$ and $\delta\omega = 0.2$. Top-left panel: radial profile of the θ-averaged angular velocity (sub-panel (a)), normalised to the Keplerian angular velocity $\Omega_\star$, and of the ratio $\ell/\ell_{\rm K}$ of the θ-averaged specific angular momentum over the Keplerian one for the same mass distribution (sub-panel (b)). Solid, dashed, dotted, and dash-dotted lines correspond to $|\beta| = 1$, 4, 8, 16, respectively. The solid thin line in sub-panel (a) shows the Keplerian angular velocity. Bottom-left panel: percentage excess of rotation relative to the polar angular velocity as a function of radius at constant latitude $\theta_{\rm lat}$. Solid, dashed, and dotted lines correspond to $\theta_{\rm lat} = 0°$ (equator), 30°, and 60°, respectively, while thin and thick lines refer to $|\beta| = 1$ and $|\beta| = 16$. Right panel: 2D maps of the internal relative excess of angular velocity relative to the polar rotation for $|\beta| = 1$ and $|\beta| = 16$. Note that the surface rotation of both maps is the same.

velocity $\Omega_{\rm K}(r) = \sqrt{GM(r)/r^3}$ associated to the same mass distribution. Outside $\sim 0.2\ R_\star$, $\Omega_{\rm K}$ grows inward as $r^{-3/2}$ (since most of the mass of the envelope is contained in the central core), faster than $\langle\Omega\rangle$. Then, it slightly flattens, but it suddenly starts to grow again as $r^{-3/2}$ due to the presence of the central black hole that dominates the enclosed mass ϕ out to $\sim 0.02R_\star$, resulting in $\Omega_{\rm K} \gg \langle\Omega\rangle$ at r_0.

Although convection can induce solid body rotation, this is not achieved in the entire envelope, but only in the central part. This is shown in the lower-left panel of Figure 2, where we plot the radial profiles of Ω (shown as the percentage excess of rotation compared to the surface angular velocity at the poles $\omega_\star$) at different latitudes $\theta_{\rm lat}$ ($\theta_{\rm lat} = 0°$ means the equator). Most of the stellar volume is differentially rotating at different latitudes, as shown by the two extreme examples $|\beta| = 1$ and $|\beta| = 16$. Those are representative of the two limiting cases: when $|\beta| \to 0$, the angular velocity becomes constant on cylinders. This can be seen in the region close to the surface around the equator of the map corresponding to $|\beta| = 1$. At constant latitude, Ω decreases as r goes from the surface to $\sim 0.3 - 0.4R_\star$, when it starts to mildly grow inward and it becomes nearly constant within $\sim 0.1R_\star$; then, it steepens again close to the central black hole. On the other hand, when $|\beta| \gg 1$, the angular velocity tends to be "shellular", i.e. it mostly follows the isobars and Ω varies with r only. That can be seen in the example map for $|\beta| = 16$ within $\sim 0.5R_\star$, while in the outermost parts of the star the angular velocity maintains a net θ-dependency and it quickly grows as r decreases.

The ratio $\ell/\ell_{\rm K}$ between the specific angular momentum ℓ and the Keplerian angular momentum for the same mass distribution closely relates to $\langle\Omega\rangle$ and $\Omega_{\rm K}$, as shown in the top-left panel (sub-panel (b)). Outside $\sim 0.2R_\star$, $\ell/\ell_{\rm K}$ first decreases inward, then flattens till $\sim 0.02R_\star$, to decrease again roughly as $\propto r^{3/2}$. Finally, within $0.005R_\star$, the ratio decreases inward more slowly, as a consequence of the steepening of $\langle\Omega\rangle$ close to the central black hole (Figure 2). Close to r_0, $\ell/\ell_{\rm K}$ typically assumes values $\sim 10^{-4}$, with mild variations within a factor $\gtrsim 2$ when $|\beta|$ is changed between 1 and 16, suggesting that the exact value of $|\beta|$ has a minor impact on the ratio $\ell/\ell_{\rm K}$ at about r_0.

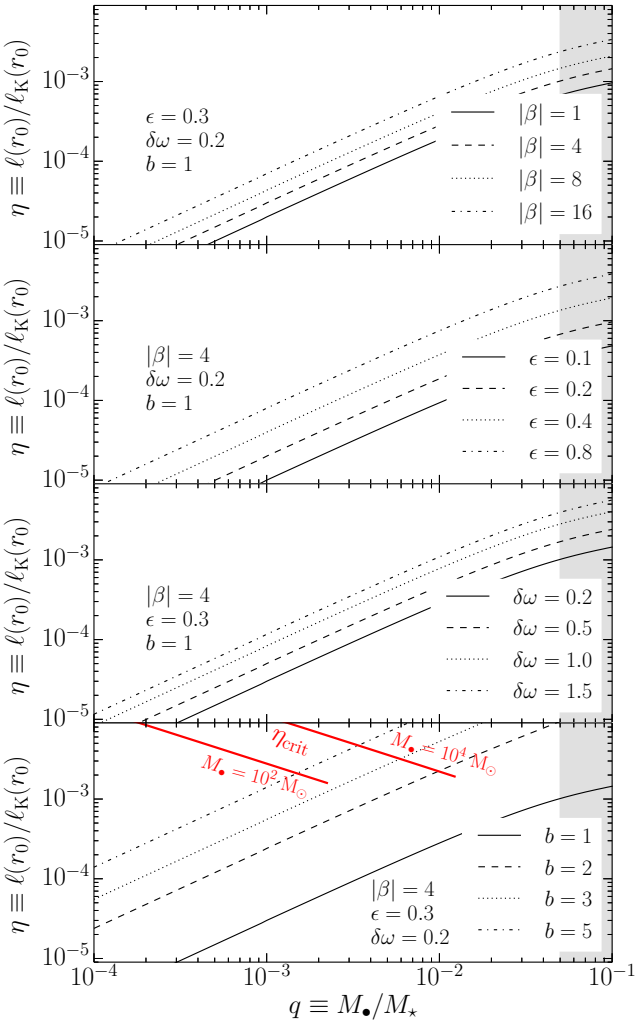

Figure 3. Ratio $\ell/\ell_{\rm K}$ of the specific angular momentum over the Keplerian one at r_0 as a function of q for different parameters. From top to bottom: the effect of changing β, ϵ, $\delta\omega$, and b. The lower panel also shows two example curves (red continuous lines) for $\eta_{\rm crit}$ (see equation 19), calculated from the models of Paper I for $M_\bullet = 10^2$ and 10^4 M$_\odot$.

The small $\ell/\ell_{\rm K}$ value at r_0 is a direct consequence of the quasi-star structure, and in particular of the presence of the central black hole. This can be better understood by comparing a quasi-star with a similar system, namely a standard $\gamma = 4/3$ polytrope with the same envelope mass, but without the central black hole. The pure polytropic structure is more compact and has a solid body rotation all the way to the centre, with a lower and nearly constant Keplerian velocity due to the absence of the black hole. This case leads to a typical ratio $\ell/\ell_{\rm K} \sim 0.1 - 0.01$ larger then in the equivalent quasi-star.

We have tested the sensitivity of $\ell/\ell_{\rm K}$ around r_0 on the structural parameters of the star: q, ϵ, $\delta\omega$, and b. Figure 3 shows that quasi-stars with proportionally larger black holes at the centre (i.e. with larger q) tend to have larger $\ell/\ell_{\rm K}$ close to r_0, though this ratio remains confined within $\sim 10^{-2}$ for $q \leq 10^{-2}$ for all the parameter combinations that we expect to bracket consistent quasi-star solutions. $\ell/\ell_{\rm K}$ departs more from $\propto r^{3/2}$ for larger q, becoming shallower close to r_0. When the quasi-star rotates proportionally faster at the equator than at the pole (i.e. when ϵ decreases and $\delta\omega$ increases) the spread between the rotation laws with different $|\beta|$ increases, but this does not change their shape and the typical $\ell/\ell_{\rm K}$ close to r_0. We note that the value of $\ell/\ell_{\rm K}$ at r_0 is mostly sensitive to b (i.e. the size of the accretion region around the black hole, see equation 1). The ratio $\ell/\ell_{\rm K}$ at r_0 grows with b as r_0 proportionally increases. Nonetheless, $\ell/\ell_{\rm K}$ always remains well below 1, reaching up to $\sim 10^{-2}$ for $b = 5$ for quasi-stars with large mass ratios $q \gtrsim 10^{-2}$.

We therefore conclude that, regardless of the strict values of the parameters assumed, the typical specific angular momentum where the gravity of the black hole starts to dominate (i.e. around r_0) is much lower than the local Keplerian angular momentum. We discuss the implications (as well as the limitations) of this result for quasi-stars in Section 3.

3 DISCUSSION AND CONCLUSIONS

3.1 Possible implications

In this paper, we investigate the role of rotation within quasi-stars. Although a fully self-consistent description of the rotating envelope is beyond the purposes of this paper, our treatment of rotation can be used to assess the coupling between the inner accretion region and the massive envelope. Before discussing the implications of our findings for black holes forming inside rotating quasi-stars, we recall their fate, when rotation is not included. This is summarised in Figure 4, adapted from Paper I, to which we refer the reader for more details. Combinations of $(M_\bullet, M_\star)$ that lie in the region marked as "No Hydrostatic Solutions" cannot form a stable envelope surrounding the black hole and therefore this latter cannot go through a phase of super-Eddington growth inside a quasi-star. For this to happen, the envelope needs to be at least a few hundred times more massive than its black hole (the parameter space marked as "Growth Region"). There, black holes with an initial mass of ~ 100 M$_\odot$ can reach in just $\gtrsim 10^4$ yr more than 10^4 M$_\odot$, depending on the initial envelope mass. This is because the black hole accretes at or beyond the Eddington rate for *the envelope mass*. Moreover, in these massive envelopes the loss of mass via winds induced by the super-Eddington luminosities proceeds at a lower rate than the black hole growth. The opposite is true for lower envelope masses at the same black hole masses within the "Evaporation Strip", where outflows remove matter from the envelope faster than black hole accretion, and the latter is then suppressed. Here a quasi-star can form, but it can just last for $< 10^4$ yr, with little impact on the embedded black hole. We can now turn our attention to a discussion on how our results might affect this picture.

In our calculations, we neglect any general relativistic effect. It is then worth comparing the Schwarzschild radius $r_{\rm s}$ of the central black hole, that sets the size of the black hole horizon, with the envelope's inner radius r_0, where our calculation stops:

$$\frac{r_{\rm s}}{r_0} = \frac{4c_{\rm s,0}^2}{bc^2} = \frac{8\left(\pi G^3\right)^{1/4}}{3\,c^2}\,\frac{M_\bullet^{1/2}\,P_0^{1/4}}{b\,\phi_0^{1/2}} \approx \approx 5.2\times10^{-8}\,b^{-1}\,q^{-1/2}\,m_\bullet^{1/2}\,p_{0,8}^{1/4}\,, \quad (17)$$

where we used $\phi_0 \approx 2q$. Inserting consistent mass-pressure values from the models shown in Figure 4 we typically find that r_0 is between a few to several thousand Schwarzschild radii of the black hole. For example, when we consider the Growth Region and take (i) a relatively small quasi-star, ($M_\bullet = 100$ M$_\odot$, $M_\star = 2\times10^5$ M$_\odot$ and $P_0 = 6.3\times10^{10}$ erg cm^{-3}); and (ii) a massive quasi-star with a relatively more massive black hole,

($M_\bullet = 10^4\ \mathrm{M}_\odot$, $M_\star = 10^7\ \mathrm{M}_\odot$ and $P_0 = 3.4\times10^{10}$ erg cm^{-3}), we find $r_\mathrm{s}/r_0 \approx 1.2\times10^{-4}$ and $r_\mathrm{s}/r_0 \approx 7.1\times10^{-4}$, respectively. These estimates support our choice of neglecting any general relativistic effect and we can therefore safely use our results at r_0 to put boundary conditions to the central accretion flow.

Although a detailed modelling of the central accretion flow is beyond the purpose of this work, we can still gain insight into its formation and some possible features from simple inferences from our results. The results of Section 2.3 suggest that the specific angular momentum at r_0 is $\ell_0 = \eta\,\ell_\mathrm{K}(r_0)$, where η is $\sim 10^{-3} - 10^{-4}$. By assuming the conservation of angular momentum, we can calculate the circularisation radius r_circ around the central black hole, i.e. the radius at which ℓ_0 corresponds to a circular orbit:

$$\frac{r_\mathrm{circ}}{r_0} = \eta^2, \tag{18}$$

where we assume that $\Omega \simeq \Omega_\mathrm{K}$ below r_0, as the black hole's gravity dominates. This radius tells us the scale below which some sort of accretion disc may eventually form. That requires $r_\mathrm{circ} > r_\mathrm{isco} \approx r_\mathrm{s}$, where r_isco is the radius of the innermost stable circular orbit, which is a few times r_s, depending on the black hole spin. We can combine equation (17) and (18) to determine a condition on η,

$$\begin{aligned}\eta \;&>\; \eta_\mathrm{crit} = \left[\frac{8\,(\pi G^3)^{1/4}}{3\,c^2}\right]^{1/2} \frac{M_\bullet^{1/4} P_0^{1/8}}{b^{1/2}\phi_0^{1/4}} \approx \\ &\approx\; 1.3\times10^{-2}\, b^{-1/2}\, q_{-4}^{-1/4}\, m_{\bullet,100}^{1/4}\, p_{0,10}^{1/8},\end{aligned} \tag{19}$$

where $q = q_{-4}\times10^{-4}$, $M_\bullet = m_{\bullet,100}\times100\ \mathrm{M}_\odot$, and $P_0 = p_{0,10}\times10^{10}$ erg s^{-1}. When $\eta > \eta_\mathrm{crit}$, the gas circularisation is such that $r_\mathrm{circ} > r_\mathrm{isco}$ and an accretion disc can form at the centre of a quasi-star. As an example, we calculate η_crit for the same quasi-star models used above, and find that $\eta_\mathrm{crit} \approx 1.1\times10^{-2}$ and $\eta_\mathrm{crit} \approx 2.7\times10^{-2}$, respectively. Those numbers are also representative of the whole Growth Region, as they weakly depend on q, $M_\bullet$ and P_0 (see equation 19). Interestingly, $\eta_\mathrm{crit} \gtrsim 10^{-2}$ is comfortably larger than the indicative upper limit on $\eta \sim$ a few $\times\,10^{-3}$ that we estimate in Section 2.3, leading to the conclusion that typical quasi-stars in the Growth Region might *not* be able to develop an accretion disc at their centre.

To better assess this point, we exploit the models used to construct Figure 4 to thoroughly explore the parameter space. Specifically, we take the values of $M_\bullet$, $M_\star$ (hence q), and P_0 (calculated at $r_0 = 5r_\mathrm{B}$) and we use them to calculate η and η_crit across the $M_\bullet - M_\star$ plane. As discussed in Section 2.3, the value of η depends on some parameters, namely $(|\beta|, \epsilon, \delta\omega)$. We tested several configurations: (i) a "fiducial" model with $(4.5, 0.5, 0.2)$, (ii) a model with a higher value for $|\beta|$, $(12, 0.5, 0.2)$, (iii) a rapidly and differentially rotating quasi-star with $(4.5, 0.1, 7.0)$, and (iv) a slowly rotating quasi-star with $(4.5, 0.1, 0.2)$. In all cases, we find that for each $M_\bullet$ there is an upper limit on the mass of the envelope above which the condition $\eta > \eta_\mathrm{crit}$ is not satisfied, i.e. a rotationally-supported accretion flow cannot form. These limits are shown as thick solid lines with downward pointing arrows in Figure 4. We note that the higher limits correspond to faster surface rotation and larger values of $|\beta|$. Fitting the upper limit lines, we obtain that a disc *cannot* form for:

$$M_\star \gtrsim 0.9 - 1.3\times10^5\ \mathrm{M}_\odot \left(\frac{M_\bullet}{100\ \mathrm{M}_\odot}\right)^{0.82}, \tag{20}$$

where the ≈ 0.7 uncertainty factor accounts for differences due to the parameters described above. It is very interesting to note that most of the allowed region coincides with the Evaporation Strip

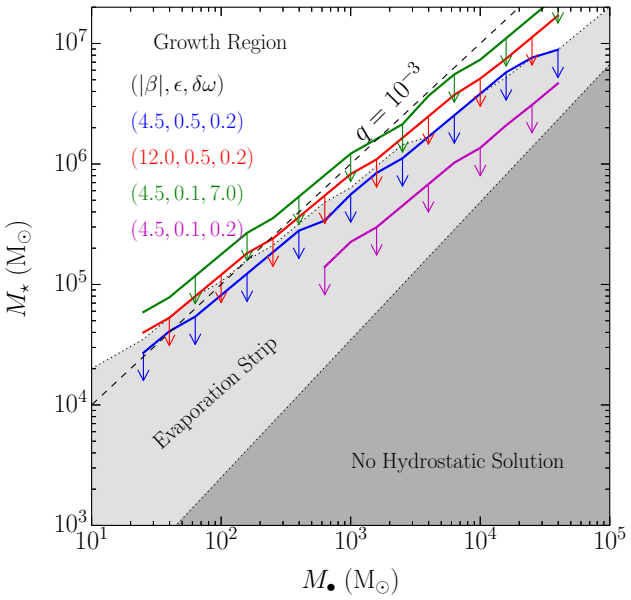

Figure 4. $M_\bullet - M_\star$ plane for quasi-stars, divided in three regions: the growth region (white), the evaporation strip (light grey), and the no-hydrostatic solution region (dark grey). Blue, red, green and magenta continuous lines show the upper limits on $M_\star$ as function of $M_\bullet$ for different choices of parameters, namely $(|\beta|, \epsilon, \delta\omega) = (4.5, 0.5, 0.2)$, $(12, 0.5, 0.2)$, $(4.5, 0.1, 7)$, and $(4.5, 0.1, 0.2)$, respectively. Above this limits, which are computed from the models of Paper I, the condition $\eta > \eta_\mathrm{crit}$ is not satisfied. For reference, the black dashed line corresponds to $q = 10^{-3}$.

(where the black hole has no time to grow), while the Growth Region (where the central black hole could quickly grow to large masses) is almost entirely excluded. The sub-linear scaling in equation (20), close to the lines of constant q, is the result of the dependence[2] of η on q, combined with the milder dependence of η_crit on q and on the properties of the quasi-star.

The models of Figure 4 have been calculated using $b = 5$ (see Paper I). As we show in the lowest panel of Figure 3, this represents the most favourable case for the formation of a central accretion disc. For $b = 2$ or 3, the value of η crosses η_crit only for central black holes with mass $\gtrsim 10^4\ \mathrm{M}_\odot$, while for $r_0 = r_\mathrm{B}$ this does not happen for any mass ratio. Therefore, in this last case, quasi-stars might not even form in the Evaporation Strip.

Our conclusions might affect the evolution of quasi-stars. An accretion disc is required as it provides an efficient source of luminosity to sustain the envelope through transport of angular momentum and the extraction of gravitational potential energy (e.g. via magneto-rotational instability; Balbus & Hawley 1991). If a rotationally-supported disc cannot form, we would be in the presence of an optically-thick, quasi-radial flow, that would nearly follow a Bondi-like accretion flow, if well within the trapping radius (Begelman 1978, 1979). In this case, within the Bondi radius, the gas becomes supersonic and almost free-falling, converting most of the gravitational potential energy into kinetic energy and little into

[2] As it can be noticed from equation (13), the shape of the Ω contours depends mostly on q for different quasi-stars, being β constant as physically estimated in Section 2.2. See also Figure 3.

internal energy that could be eventually radiated or convectively transported outward. Since the black hole has no surface, this kinetic energy cannot be dissipated and is advected into the black hole. Even assuming a dissipation mechanisms within the flow, most of the radiation produced would be dragged inward and swallowed by the black hole (Begelman 1979; Alexander & Natarajan 2014). Therefore, a consistent model for a quasi-star seems not to exist in the Growth Region of the parameter space of Figure 4.

Stepping onto more speculative grounds, we may foreseen a possible fate for supermassive black holes that might form in such conditions. According to recent numerical and analytical calculations, when a very massive star ($\gtrsim 10^5$ M$_\odot$) forms as consequence of a high accretion rate of gas ($\gtrsim$ 1 M$_\odot$ yr^{-1}), its inner core eventually collapses, presumably into a small ($\sim$ 100 M$_\odot$) black hole (Begelman 2010; Hosokawa et al. 2013). At this point, however, our results suggest that the surrounding mass might start to be radially accreted, unimpeded by the black hole energy feedback. Since there is no maximum limit for the accretion rate onto a black hole (there is only a limit in luminosity), this may lead to a phase of super-exponential accretion (Alexander & Natarajan 2014). The process will stop when/if the angular momentum in the accretion flow increases outward so that the circularisation radius increases faster than the black hole's $r_{\rm isco}$. The outcome clearly depends on the exact hydrodynamics of the flow, but direct formation of massive seeds $\gtrsim 10^5$ M$_\odot$ might be in principle possible. In this scenario, limiting factors for the black hole seed mass would be linked to the galaxy ability to funnel and accumulate pristine gas in its centre: low cosmological gaseous inflow rate, non efficient angular momentum redistribution and copious star formation (Latif et al. 2013a; Choi et al. 2013, 2015).

Small black holes born in the Evaporation Strip might face a different fate. There, an accretion disc can still form, but the available angular momentum is usually low, such that dissipation should occur very close to the black hole. One may therefore speculate that a quasi-spherical, geometrically-thick, radiation-dominated accretion disc, such as a "ZEBRA" (ZEro-BeRnoulli Accretion flow; Coughlin & Begelman 2014) can form. Therefore, we have tried to smoothly join the ZEBRA with the envelopes of the models from Paper I at the inner radius r_0. First, we note that $\eta^2 = \ell_0^2/\ell_{\rm K}^2(r_0)$ corresponds to the normalisation of the specific angular momentum of the gas "a" (see equation (10) in Coughlin & Begelman 2014). Given $\gamma = 4/3$, this only depends on the radial slope n of the mass flow within the ZEBRA (i.e. $\dot{M} \propto r^n$), which is the main structural parameter of the model. Since the ZEBRA should form in the central region of the envelope within r_0, we assume that its external radius $\mathcal{R} = r_0$. Finally, we normalise the density by requiring that the luminosity transported by convection outward through the ZEBRA envelope, i.e. $L_{\rm adv} \approx 4\pi\mathcal{R}^2 P(\mathcal{R}) c_{\rm s}(\mathcal{R}) = 4\pi\mathcal{R}^2 P_0 c_{\rm s,0}$, is equal to the central luminosity $L_\bullet$ required to self-consistently sustain the envelope. Unfortunately, we find no consistent solutions where the accretion disc is less massive than the black hole, as it is envisaged in the original model. We would therefore need an extension of this model to self gravitating disc, to assess its viability in our case. Another possibility is to relax the requirement that $L_{\rm adv} = L_\bullet$ and speculate instead that $L_\bullet$ is provided by partially tapping the energy funnelled into a powerful jet, whose presence is foreseen in the ZEBRA model. However, the jet is likely going to pierce the envelope, behaving as an outlet of energy, and therefore how enough energy could be transferred in a gentle, uniform way to the envelope is unclear, though possible in principle.

Nonetheless, even if it would be possible to inject within the quasi-star the required luminosity at/above the Eddington limit for the whole mass, the evaporation of the envelope would anyway prevent substantial accretion to occur. Therefore, there might be two populations of supermassive black hole seeds from direct collapse via supermassive stars: one extremely massive, say $> 10^{4-5}$ M$_\odot$ in massive haloes $\gtrsim 10^{8-9}$ M$_\odot$, and one extremely light $\sim$ 100 M$_\odot$ in more common haloes at the epoch of formation ($z \sim 15$). This possibility represents also a "smooth" transition between scenarios of light-seed formation based on PopIII stars and massive-seed formation based on direct collapse.

3.2 Limitations of our treatment

Though intriguing and possible in principle, the speculations discussed in Section 3.1 relay on results strongly dependent on the assumed model for the quasi-star hydrostatic structure and rotation. We therefore comment on the limitations of this model.

The simplified description of the quasi-star internal structure as a loaded polytrope (which is unrelated to rotation) requires three parameters to be specified, namely the central pressure P_0, the black hole mass $M_\bullet$ and the mass of the envelope $M_\star$ through the ratio q. However, this neglects the energy production mechanism at the centre, which would introduce an additional relation between e.g. P_0 and $M_\star$, leaving only two parameters to describe the model with simple scalings (e.g. equations (8)-(10) from Dotan et al. 2011). Nonetheless, this treatment provides the correct estimates as long as, for each $M_\bullet - q$ pair, P_0 is chosen consistently with detailed equilibrium models[3] (e.g. Paper I).

We model the rotation inside the convective envelope of a quasi-star using the model proposed by Balbus et al. (2009) and Balbus & Weiss (2010). Despite the remarkable agreement with the available data of the internal rotation in the solar convective zone and the physical argumentations supporting its reliability, there are no *a priori* reasons why this model should apply within a quasi-star nor it should produce a sensible description of its rotation, specially at its centre. However, we can test the fundamental assumption behind it, namely that convective cells are long lived compared to the rotation period $t_{\rm rot} \sim 2\pi(\epsilon\Omega_{{\rm K},\star})^{-1}$. Since convection produces subsonic motions without net mass redistribution, a rough lower limit for the lifetime of a convective element could be $t_{\rm conv} \sim R_\star/c_{\rm s,0}$. However, we can obtain a better estimate by applying the mixing length theory (e.g. Böhm-Vitense 1958), which leads to $t_{\rm conv} \sim \sqrt{\alpha\, h_P/(g\delta)}$, where $\alpha \sim 1-2$ is the mixing length parameter[4] (Asida 2000; Girardi et al. 2000; Palmieri et al. 2002; Ferraro et al. 2006), h_P is the pressure scale-height, $g \sim GM_\star/R_\star^2$ is the gravitational field, and $\delta = \Delta T/T$ is the relative (positive) deviation of the temperature gradient from the adiabatic one in convective regions. The latter is usually tiny, ranging from $\sim 10^{-5}$ to $\sim 10^{-8}$ in deep convective zones (e.g. Böhm-Vitense 1992; Chabrier et al. 2007; Prialnik 2009), and in fact it justifies the description of convective regions through adiabatic relations. Comparing convection and rotation timescales, we

[3] Since the self consistent models solve for the energy transport, choosing a consistent value of P_0 given $M_\star$ and $M_\bullet$ is then implicitly equivalent to consider the energy transport within the star. Moreover, the convective envelope of equilibrium models is formally obtained by solving the equations of a loaded polytrope, and since it dominates the mass and volume of the stars, it provides alone a remarkable description of the entire hydrostatic structure.

[4] Mixing-lenght theory assumes that convective cells live and mix over a mean free path $l = \alpha h_P$, where α is a free parameter (Böhm-Vitense 1958).

obtain:

$$\frac{t_{\rm conv}}{t_{\rm rot}} \sim \frac{\epsilon\sqrt{\alpha}}{2\pi}\left(\frac{h_P}{R_\star\delta}\right)^{1/2} \sim 3.6\,\epsilon_{0.5}\,\delta_{-5}^{-1/2}\,(h_P/R_\star)_{-2}^{1/2}, \quad (21)$$

where $\epsilon = 0.5\epsilon_{0.5}$, $\alpha = 2$, $\delta = 10^{-5}\delta_{-5}$, and $h_P/R_\star = 10^{-2}(h_P/R_\star)_{-2}$, as we typically find $h_P/R_\star \gtrsim 0.01$ in the convective envelope of the models of Paper I. This order of magnitude calculation suggests that our model should be reasonably applicable to quasi-stars since the convection timescale is at least comparable or even longer than the rotation period, making convective features long-lived enough to couple with and lie along constant Ω contours.

The derivation of equation (5) formally requires the assumption that rotation is weak, i.e. that departures from sphericity in the hydrostatic equilibrium equation are negligible. In fact, this assumption enters only in the final substitution $(1/\rho)\partial P/\partial r \rightarrow -{\rm d}\Phi/{\rm d}r$, but it would generally hold in the central regions we are interested in. Indeed, simple calculations show that the ratio between the centrifugal and the gravitational force becomes smaller toward radii $r \ll R_\star$ for any reasonable density profile and angular velocity with a radial scaling shallower than the Keplerian one (see also e.g. Chandrasekhar 1933; Monaghan & Roxburgh 1965). Therefore, we conclude that the assumption of weak rotation is not crucial for our findings.

Our model describes a steady-state configuration (thought to be an average in time), whose velocity field is dominated by the azimuthal component, i.e. rotation itself. However, convective regions in differentially rotating zones might lead to features that this approach cannot capture, such as meridional circulation and convective turbulence (e.g. Browning et al. 2004; Ballot et al. 2007; Browning 2008; Featherstone & Miesch 2015). Those processes are though to be relevant, especially when coupled with magnetic fields, to understand the long-term maintenance and the mutual powering of the differential rotation and the magnetic dynamo within the Sun. In our case, they might be relevant in the redistribution of angular momentum within the convective envelope, possibly having an effect on the rotation of the central region.

Finally, we recall that quasi-stars are thought to be accreting at high rates ($\gtrsim 1$ M$_\odot$ yr^{-1}) from the local environment. That means that quasi-stars may not be steady rotating objects, as assumed by our model. Moreover, accretion from outside may proceed either from a surrounding disc, especially when small scale turbulence is accounted for (Latif et al. 2013a), or in a more disordered fashion from filamentary structures carrying angular momentum with various orientations and amplitudes (Choi et al. 2015). In both cases, gravitational torques from non-axisymmetric features might play a relevant role in influencing the redistribution of angular momentum within the quasi-star envelope, though we cannot explicitly account for that in the present work by assuming a steady-state, temporarily-averaged rotation.

3.3 Direct collapse haloes

We now attempt to identify the haloes that could host a supermassive star $M_\star \gtrsim 10^5$ M$_\odot$. First, we require that $\dot{M} \gtrsim 0.1$ M$_\odot$ yr^{-1}, as needed to assemble $M_\star$ within $\sim 1-2$ Myr, i.e. the lifetime of a supermassive star (Begelman 2010; Hosokawa et al. 2013). The supermassive star may accrete either gas transported through the protogalactic disc or from cosmological inflows onto the halo, proceeding all the way down to the centre as cold flows (e.g. Di Matteo et al. 2012). The latter case can be translated in a lower limit on the redshift z at which a halo $M_{\rm h}$ can accrete at $\dot{M} > 0.1$ M$_\odot$ yr^{-1} through the relation[5] (Dekel et al. 2009):

$$\dot{M} \approx 75\left(\frac{f_{\rm b}}{0.16}\right)\left(\frac{1+z}{3}\right)^{2.25}\left(\frac{M_{\rm h}}{10^{12}\ {\rm M}_\odot}\right)^{1.15}\ {\rm M}_\odot\ {\rm yr}^{-1}, \quad (22)$$

where $f_{\rm b}$ is the cosmic baryon fraction. We follow Schneider (2015) to calculate the collapse redshift of the halo, i.e. the redshift $z_{\rm col}$ at which a fraction F of the mass $M_{\rm h}$ at redshift $\tilde{z}$ is assembled, by solving the following equation for $z_{\rm col}$:

$$\frac{1}{D(z_{\rm col})} = \frac{1}{D(\tilde{z})} + \sqrt{\frac{\pi}{2}}\frac{\sqrt{\sigma^2(FM_{\rm h}) - \sigma^2(M_{\rm h})}}{\delta_{\rm c,0}}, \quad (23)$$

where $D(z)$ is the linear growth factor ($D(0) = 1$), $\delta_{\rm c,0} = 1.686$, and $\sigma^2(M)$ is the present-day variance of the matter density field (i.e. the integral of the linear matter power spectrum over the wavenumber k) at mass scale M (for additional details, see Schneider 2015). Assuming $F = 0.05$, Figure 5 shows $z_{\rm col}$ as a function of $M_{\rm h}$ for two values of $\dot{M}$. We adopt the cosmological parameters from the latest Planck results (Planck Collaboration et al. 2015) and we find differences within a factor 2 when we vary F from 0.05 to 0.5.

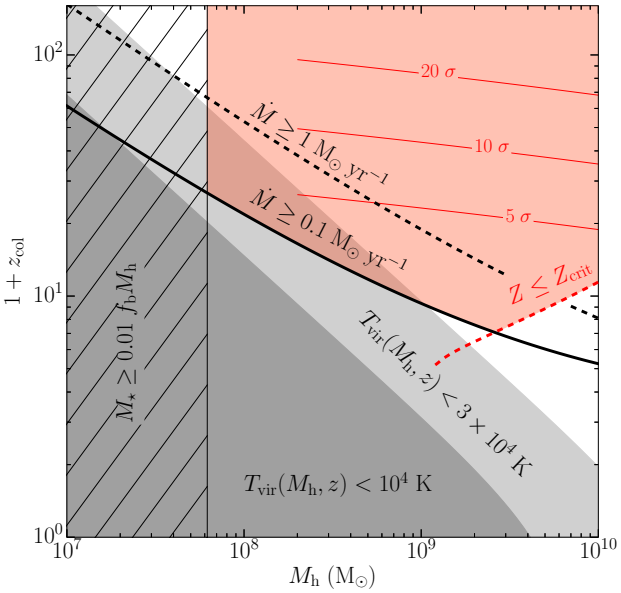

Figure 5. Redshift of collapse $z_{\rm col}$ (defined by $F = 0.05$) as a function of the halo mass $M_{\rm h}$. The continuous and dashed lines refer to $\dot{M} = 0.1$ and 1 M$_\odot$ yr^{-1}, respectively. The dark and light grey regions mark where the halo virial temperature $T_{\rm vir} < 10^4$ K and $T_{\rm vir} < 3\times10^4$ K, respectively. The hatched region marks the halo masses for which a supermassive star $M_\star = 10^5$ M$_\odot$ represents more than 1% of the baryonic mass $f_{\rm b}M_{\rm h}$. The red dashed line marks the redshift threshold above which a halo $M_{\rm h}$ has $Z < Z_{\rm cr}$ after collapsing. The red shaded region shows where supermassive stars $> M_\star$ could form in the $M_{\rm h} - z_{\rm col}$ plane, and the thin red lines denotes when haloes represent 5, 10, and 20 σ over-density fluctuations.

[5] The usage of equation (22) assumes that the gas accretion rate onto the halo is comparable to that onto the forming supermassive star. However, different assumptions for $\dot{M}(z, M_{\rm h})$ (e.g. Jeans mass collapse over the dynamical time $\dot{M} = c_{\rm s}^3/G$ at the virial temperature $T_{\rm vir}$) do not significantly change the result. Yet, we caution that this approach, in order to keep the calculations simple, neglects the possibility that the supermassive star is at the centre of a protogalaxy.

As a second constraint, we require a metallicity below $\log(Z_{\rm cr}/Z_\odot) = -3.8$, where $Z_\odot$ is the solar metallicity and the critical value roughly corresponds to the transition from PopIII to second population stars (Valiante et al. 2016). We impose this condition by using the stellar mass-metallicity relation as a function of time determined by Savaglio et al. (2005), and then connecting the stellar mass to $M_{\rm h}$ through the halo mass-stellar mass relation from Moster et al. (2013). After computing the redshift of collapse, we obtain a lower limit $z_{\rm col}(M_{\rm h})$ for haloes $M_{\rm h}$ that have $Z < Z_{\rm cr}$ by the end of the collapse. Finally, the supermassive star cannot be larger than a fraction f of the baryonic mass of the halo, namely $M_{\rm h} > M_\star/(f_{\rm b} f)$, where $f \sim 0.01$. The value of f is chosen in fair agreement with the results of cosmological simulations of the collapse of massive clouds at the centre of dark matter haloes with virial temperature $T_{\rm vir} \gtrsim 10^4$ K (e.g. Regan & Haehnelt 2009; Latif et al. 2013b; Choi et al. 2015).

The red shaded region in Figure 5 shows where all these conditions are satisfied in the $M_{\rm h} - z_{\rm col}$ plane. We also compare this region with those occupied by haloes with virial temperature $T_{\rm vir} < 10^4$ K and $T_{\rm vir} < 3 \times 10^4$. The virial temperature is calculated as $T_{\rm vir} \approx (G M_{\rm h} H \sqrt{\Delta/54})^{2/3} \mu m_{\rm p}/k_{\rm B}$, where $k_{\rm B}$ is the Boltzmann constant, $m_{\rm p}$ is the proton mass, $\mu \approx 0.59$ is the mean molecular weight for ionised hydrogen, $H(z)$ is the Hubble parameter, and $\Delta(z)$ is the z-dependent virial over-density (Bryan & Norman 1998).

The latest haloes that might be able to host a supermassive star $M_\star > 10^5$ M$_\odot$ collapse at $z_{\rm col} \sim 6.5$ and have masses $M_{\rm h} \sim 2 - 3 \times 10^9$ M$_\odot$. Those objects represents $\sim 2\sigma$ peaks in the matter density distribution and have typical comoving number densities $\sim 0.6 - 0.9$ cMpc^{-3} dex^{-1}. Supermassive stars can also form within both heavier and lighter haloes virtually at any redshift $z_{\rm col} > 10$, when they are able to sustain the inflow and the gas is still pristine enough. However, beyond $z_{\rm col} \sim 20$, the candidate hosts of supermassive stars more massive than 10^5 M$_\odot$ becomes extremely rare, representing more than 5σ over-density fluctuations of the matter density field. Therefore, we can grossly identify the hosts of supermassive stars possibly leading to the formation of $\sim 10^{4-5}$ M$_\odot$ back hole seeds as dark mater halos with masses about $\sim 10^9$ M$_\odot$, collapsing between $z \sim 20$ and $z \sim 10$, in agreement with previous results (e.g. Begelman et al. 2006; Volonteri & Begelman 2010; Valiante et al. 2016). However, we note that our approach (i) requires to extrapolate the used relations to relatively high z, and (ii) it does not account for environmental effects (e.g. the proximity of a massive halo producing H_2-dissociating Lyman-Werner photons), therefore the limits above should be taken as approximated.

3.4 Summary and conclusions

In this paper, we make a first attempt to discuss possible effects that rotation may have on the structure and evolution of quasi-stars. Specifically, we have addressed the issue of whether the redistribution of angular momentum inside the convective envelope of a quasi-star in steady rotation may favour the formation of a central accretion disc. We adopt a model developed initially by Balbus et al. (2009) and then improved in a sequence of more recent papers by the same authors to describe the distribution of angular momentum within the convective zone of the Sun and we apply it to quasi-stars.

Within the limitations of this approach (discussed in Section 3.2), we find that, at given $M_\bullet$, most of the massive quasi-stars might not be able to form a central, rotationally-supported accretion region, while the contrary is true for lower mass quasi-stars, typically living within the Evaporation Strip. This bimodal behaviour could lead to different fates, depending on the mass of the original supermassive star at the collapse of the central core that leads to the formation of the central embryo black hole. At high masses, the black hole might swallow most of the mass that is still infalling from larger radii without providing enough feedback either to stabilise the structure or to halt the collapse. The central black hole would then accrete a large fraction of the envelop mass, possibly reaching $M_\bullet \sim 10^{4-5}$ M$_\odot$. On the other hand, less massive envelopes might be able to form a central accretion disc and to reach an equilibrium configuration, i.e. a quasi-star. However, outflows then suppress the growth of the central black hole, leading to $M_\bullet \sim 10^{2-3}$ M$_\odot$.

Our results are therefore intriguing, implying possible alternative outcomes for the formation of supermassive black hole seeds by direct collapse. However, this potential needs to be further scrutinised with detailed numerical simulations, as the limitations of our analytical treatment suggest caution. Nonetheless, our first exploration still recommends that further work should be devoted during the future to the topic of rotation within supermassive and quasi-stars, since it might be instrumental to better understand crucial details of the formation process of massive black hole seeds via direct collapse.

ACKNOWLEDGEMENTS

We thank the anonymous Referee for useful comments that helped us improve the quality of this work. We thank Mitch Begelman, Lucio Mayer and Athena R. Stacy for useful discussions and for a thorough reading of this manuscript in the draft phase. D.F. is supported by the Swiss National Science Foundation under grant #No. 200021_140645.

REFERENCES

Agarwal B., Smith B., Glover S., Natarajan P., Khochfar S., 2015, preprint, (arXiv:1504.04042)
Alexander T., Natarajan P., 2014, Science, 345, 1330
Asida S. M., 2000, ApJ, 528, 896
Balbus S. A., 2009, MNRAS, 395, 2056
Balbus S. A., Hawley J. F., 1991, ApJ, 376, 214
Balbus S. A., Latter H. N., 2010, MNRAS, 407, 2565
Balbus S. A., Schaan E., 2012, MNRAS, 426, 1546
Balbus S. A., Weiss N. O., 2010, MNRAS, 404, 1263
Balbus S. A., Bonart J., Latter H. N., Weiss N. O., 2009, MNRAS, 400, 176
Balbus S. A., Latter H., Weiss N., 2012, MNRAS, 420, 2457
Ball W. H., Tout C. A., Żytkow A. N., Eldridge J. J., 2011, MNRAS, 414, 2751
Ball W. H., Tout C. A., Żytkow A. N., 2012, MNRAS, 421, 2713
Ballot J., Brun A. S., Turck-Chièze S., 2007, ApJ, 669, 1190
Baumgarte T. W., Shapiro S. L., 1999, ApJ, 526, 941
Begelman M. C., 1978, MNRAS, 184, 53
Begelman M. C., 1979, MNRAS, 187, 237
Begelman M. C., 2010, MNRAS, 402, 673
Begelman M. C., Shlosman I., 2009, ApJ, 702, L5
Begelman M. C., Volonteri M., Rees M. J., 2006, MNRAS, 370, 289
Begelman M. C., Rossi E. M., Armitage P. J., 2008, MNRAS, 387, 1649
Böhm-Vitense E., 1958, Z. Astrophys., 46, 108
Böhm-Vitense E., 1992, Introduction to stellar astrophysics. Volume 3. Stellar structure and evolution.
Bromm V., Loeb A., 2003, ApJ, 596, 34
Brott I., et al., 2011, A&A, 530, A115

Browning M. K., 2008, ApJ, 676, 1262
Browning M. K., Brun A. S., Toomre J., 2004, ApJ, 601, 512
Bryan G. L., Norman M. L., 1998, ApJ, 495, 80
Chabrier G., Gallardo J., Baraffe I., 2007, A&A, 472, L17
Chandrasekhar S., 1933, MNRAS, 93, 390
Choi J.-H., Shlosman I., Begelman M. C., 2013, ApJ, 774, 149
Choi J.-H., Shlosman I., Begelman M. C., 2015, MNRAS, 450, 4411
Coughlin E. R., Begelman M. C., 2014, ApJ, 781, 82
Dekel A., Sari R., Ceverino D., 2009, ApJ, 703, 785
Devecchi B., Volonteri M., 2009, ApJ, 694, 302
Devecchi B., Volonteri M., Rossi E. M., Colpi M., Portegies Zwart S., 2012, MNRAS, 421, 1465
Di Matteo T., Khandai N., DeGraf C., Feng Y., Croft R. A. C., Lopez J., Springel V., 2012, ApJ, 745, L29
Dijkstra M., Ferrara A., Mesinger A., 2014, MNRAS, 442, 2036
Dotan C., Rossi E. M., Shaviv N. J., 2011, MNRAS, 417, 3035
Eggenberger P., Miglio A., Montalban J., Moreira O., Noels A., Meynet G., Maeder A., 2010, A&A, 509, A72
Ekström S., et al., 2012, A&A, 537, A146
Fan X., et al., 2006, AJ, 131, 1203
Featherstone N. A., Miesch M. S., 2015, ApJ, 804, 67
Ferraro F. R., Valenti E., Straniero O., Origlia L., 2006, ApJ, 642, 225
Fiacconi D., Rossi E. M., 2016, MNRAS, 455, 2
Fowler W. A., 1966, ApJ, 144, 180
Girardi L., Bressan A., Bertelli G., Chiosi C., 2000, A&AS, 141, 371
Hosokawa T., Omukai K., Yorke H. W., 2012, ApJ, 756, 93
Hosokawa T., Yorke H. W., Inayoshi K., Omukai K., Yoshida N., 2013, ApJ, 778, 178
Huntley J. M., Saslaw W. C., 1975, ApJ, 199, 328
Johnson J. L., Bromm V., 2007, MNRAS, 374, 1557
Kitchatinov L. L., Ruediger G., 1995, A&A, 299, 446
Latif M. A., Schleicher D. R. G., Schmidt W., Niemeyer J., 2013a, MNRAS, 433, 1607
Latif M. A., Schleicher D. R. G., Schmidt W., Niemeyer J. C., 2013b, MNRAS, 436, 2989
Lodato G., Natarajan P., 2006, MNRAS, 371, 1813
Madau P., Rees M. J., 2001, ApJ, 551, L27
Madau P., Haardt F., Dotti M., 2014, ApJ, 784, L38
Mayer L., Fiacconi D., Bonoli S., Quinn T., Roškar R., Shen S., Wadsley J., 2015, ApJ, 810, 51
Miesch M. S., Brun A. S., Toomre J., 2006, ApJ, 641, 618
Milosavljević M., Bromm V., Couch S. M., Oh S. P., 2009, ApJ, 698, 766
Monaghan F. F., Roxburgh I. W., 1965, MNRAS, 131, 13
Mortlock D. J., et al., 2011, Nature, 474, 616
Moster B. P., Naab T., White S. D. M., 2013, MNRAS, 428, 3121
Palacios A., Charbonnel C., Talon S., Siess L., 2006, A&A, 453, 261
Palmieri R., Piotto G., Saviane I., Girardi L., Castellani V., 2002, A&A, 392, 115
Pelupessy F. I., Di Matteo T., Ciardi B., 2007, ApJ, 665, 107
Planck Collaboration et al., 2015, preprint, (arXiv:1502.01589)
Prialnik D., 2009, An Introduction to the Theory of Stellar Structure and Evolution
Quinlan G. D., Shapiro S. L., 1990, ApJ, 356, 483
Regan J. A., Haehnelt M. G., 2009, MNRAS, 393, 858
Regan J. A., Johansson P. H., Wise J. H., 2014, ApJ, 795, 137
Reinhold T., Reiners A., Basri G., 2013, A&A, 560, A4
Savaglio S., et al., 2005, ApJ, 635, 260
Schneider A., 2015, MNRAS, 451, 3117
Schönberg M., Chandrasekhar S., 1942, ApJ, 96, 161
Shibata M., Shapiro S. L., 2002, ApJ, 572, L39
Tanaka T., Haiman Z., 2009, ApJ, 696, 1798
Thompson M. J., Christensen-Dalsgaard J., Miesch M. S., Toomre J., 2003, ARA&A, 41, 599
Treister E., Schawinski K., Volonteri M., Natarajan P., 2013, ApJ, 778, 130
Valiante R., Schneider R., Volonteri M., Omukai K., 2016, MNRAS, 457, 3356
Volonteri M., Begelman M. C., 2010, MNRAS, 409, 1022
Volonteri M., Silk J., Dubus G., 2015, ApJ, 804, 148
Weigel A. K., Schawinski K., Treister E., Urry C. M., Koss M., Trakhtenbrot B., 2015, MNRAS, 448, 3167
Willott C. J., et al., 2010, AJ, 140, 546
Wu X.-B., et al., 2015, Nature, 518, 512

This paper has been typeset from a TEX/LATEX file prepared by the author.